Proceedings of the ASME 2024
International Mechanical Engineering Congress and Exposition
IMECE2024
November 17-22, 2024, Portland, OR, USA

IMECE2024-147424

MULTI-DIRECTIONAL MECHANICAL PROPERTY CHARACTERIZATION OF ADDITIVELY MANUFACTURED METAL UTILIZING WAVEFIELD ANALYSIS

Bowen Cai[1], Chuangchuang Sun[1], Rani Sullivan[1], Zhenhua Tian[2]

[1]Mississippi State University, MS State, MS
[2] Virginia Polytechnic Institute and State University, Blacksburg, VA

ABSTRACT

The advancement of additive manufacturing has significantly transformed the production process of metal components. However, the unique challenges associated with layer-by-layer manufacturing result in anisotropy in the microstructure and uneven mechanical properties of additive-manufactured metal products. Traditional testing methods often fall short of providing the precise mechanical performance evaluations required to meet industry standards. This paper introduces an innovative approach that combines a nondestructive Lamb wave sensing system with a wavenumber analysis method to characterize the mechanical properties of 3D-printed metal panels in multiple directions. Our method employs piezoelectric actuators (PZT) to generate Lamb waves and utilizes a laser Doppler vibrometer (LDV) for non-contact, two-dimensional grid acquisition of the wavefield. The anisotropic properties of the metal 3D-printed structure will be captured in the wavefield, offering an informative dataset for wavenumber analysis. The proposed analytical method includes multi-directional frequency wavenumber analysis and a least-squares-based dispersion curves regression. The integration of the above advanced analytical tools allows for the accurate characterization of the shear wave velocity and Poisson's ratio of the plate structure. This precise characterization is crucial for ensuring the structural integrity and consistent mechanical properties of 3D-printed metal components. We validated our method using a 3D-printed stainless-steel plate, demonstrating its capability to effectively characterize the multi-directional mechanical properties of additively manufactured metal plates. We expect that our method can provide a nondestructive, time-efficient, and comprehensive quality control solution for additive manufacturing across various industries.

Keywords: additive manufacturing, 3D-printed metal, wavenumber analysis, dispersion curve regression, mechanical properties characterization

1. INTRODUCTION

Over the past few decades, additive manufacturing (AM) technology has made significant strides, reshaping production methods in numerous industries such as aerospace, transportation, energy, and biomedicine [1–5]. Its benefits, including reduced development costs, high design flexibility, and the elimination of traditional machining tools, have contributed to its widespread industrial adoption [6]. Among AM technologies, metal laser powder bed fusion (L-PBF) is a rapidly advancing manufacturing technique that offers excellent mechanical properties for final end-use parts [3,7,8].

As additive manufacturing continues to evolve, it has become increasingly apparent that the variation of mechanical properties in its products is becoming more complex. Various factors, such as different process parameters, scanning and build strategies, raw materials, and changes in deformation and temperature during manufacturing, can cause global or localized changes in the mechanical properties of AM products[9]. Therefore, accurately characterizing the mechanical properties of 3D-printed metal parts is essential to ensure the reliability and safety of produced parts [10]. Traditional testing methods, such as tensile, compression, and bending tests, often fall short. These conventional techniques face challenges related to porosity, microstructural inconsistencies, and the anisotropy of additively manufactured metals [11]. Additionally, these methods are typically destructive, leading to increased costs for high-value, small-batch components.

This paper proposes an innovative method that combines nondestructive Lamb wave sensing with multi-directional frequency wavenumber analysis to characterize the multi-directional mechanical properties of 3D-printed metal plates. Compared to traditional methods, this non-destructive approach covers a broad measurement area and can measure multi-directional (360-degree) and multi-type mechanical properties (e.g., shear wave velocity and Poisson's ratio) from only one test. The effectiveness of this method has been validated on a 3D-

printed stainless-steel plate, demonstrating the potential of this study for accurate and comprehensive mechanical properties characterization of additively manufactured metal structures.

In this paper, **Section 2** describes our Lamb wave sensing system and the method for characterizing mechanical properties based on the collected data, including multi-dimensional frequency-wavenumber analysis and least-squares regression of dispersion curves. **Section 3** presents the proof-of-concept experiments conducted on a 3D-printed 316L panel. Finally, **Section 4** briefly summarizes the findings and outlines the future expectations of this study.

2. TIME-SPACE WAVEFIELD ACQUISITION AND ANALYSIS

This section first introduces the detailed process for collecting time-space wavefields using the PZT-LDV Lamb wave sensing system. Next, A multi-directional frequency-wavenumber analysis method was developed to get frequency-wavenumber spectra in all directions from the collected data. Subsequently, a least-squares curve regression method is applied to the dataset extracted from the *f-k* spectra, and the results will be compared with theoretical results to determine the test sample's mechanical properties.

2.1 PZT-LDV Lamb wave sensing system and wave-field acquisition

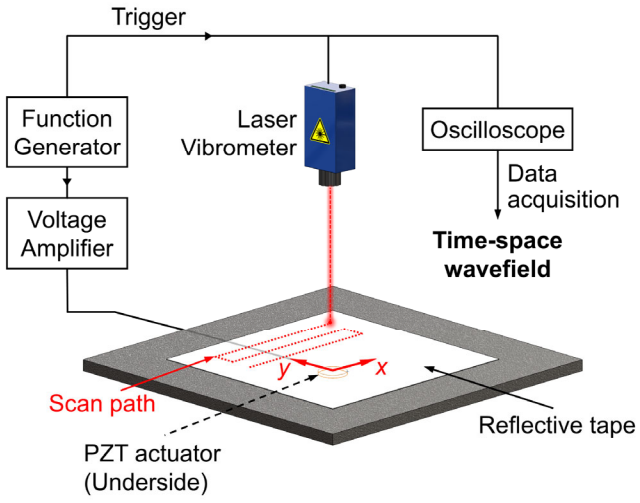

FIGURE 1: SCHEMATIC OF THE PZT–LDV LAMB WAVE SENSING SYSTEM.

Lamb waves are capable of propagating along elongated structures such as thin plates with minimal energy dissipation[12]. By measuring the surface displacement of the testing plate, it is possible to acquire a time-space wavefield of Lamb waves. Figure 1 depicts the schematic setup for the collection procedure of the time-space wavefield, detailing both the equipment used and the measurement process.

This study employs a piezoelectric transducer (PZT) combined with a laser Doppler vibrometer (LDV) to create a PZT-LDV Lamb wave sensing system. The LDV is mounted on a Computer Numerical Control (CNC) frame that can move along two axes, enabling the collection of two-dimensional Lamb wave signals with a predefined grid. The PZT actuator is driven by an amplified chirp burst from a signal generator, which initiates Lamb waves in the panel under examination. The CNC system guides the LDV to sequentially capture waveforms point-by-point along a predefined path. These waveforms are then spatially organized according to their coordinates to construct a two-dimensional time-space wavefield. The extensive data contained within this wavefield will be analyzed using multi-directional frequency-wavenumber analysis methods in the subsequent subsection.

2.2 Multi-directional frequency-wavenumber analysis

To accurately characterize the mechanical properties of the test plate, it is essential to measure the wavenumbers of Lamb waves at various frequencies and analyze their dispersion relationships. Dispersion curves are known to vary with changes in mechanical property parameters [12,13]. Therefore, to determine material properties inversely from the acquired dataset, we propose a multi-directional frequency-wavenumber analysis method to extract the frequency-wavenumber relation from the time-space wavefields.

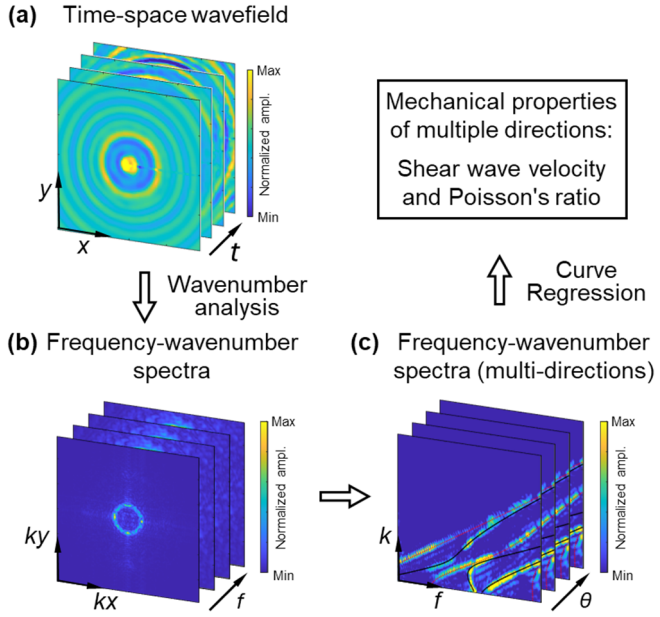

FIGURE 2: DIAGRAM OF THE MULTI-DIRECTIONAL FREQUENCY-WAVENUMBER ANALYSIS METHOD.

Figure 2 illustrates the schematic of our analysis method. The acquired time-space wavefield u (t, $\mathbf{x}$) (Fig. 2a) is a time t and position $\mathbf{x}$ function. It can be transformed into a representation in the frequency-wavenumber domain U (f, $\mathbf{k}$) (Fig. 2b) by performing a multidimensional Fourier transform [14–16]:

$$U(f,\mathbf{k}) = \int_{-\infty}^{\infty}\int_{-\infty}^{\infty} u(t,\mathbf{x}) e^{-j(2\pi ft - \mathbf{k}\cdot\mathbf{x})} dt d\mathbf{x}. \quad (1)$$

© 2024 by ASME

In this study, we will focus more on how mechanical properties are distributed in various directions. Therefore, we can reduce the spatial variables to a two-dimensional position vector, $\mathbf{x} = (x, y)$, and a wavenumber vector, $\mathbf{k} = (k_x, k_y)$. The wavenumber vector $\mathbf{k}$ at different frequencies can be represented as spatial wavenumber spectra (see Fig. 2b). These spectra reveal how wavenumber values correlate with both intensities and amplitudes across all propagation directions for guided waves and Lamb waves, respectively.

To measure the mechanical properties in each direction, the frequency-wavenumber spectra shown in Fig. 2b are segmented along various angles using radial lines originating from the center. These segmented slices facilitate the derivation of the frequency-wavenumber spectrum for each specific direction. By identifying the peak wavenumber amplitude at each frequency, an experimental dispersion curve dataset can be constructed, as shown in Fig. 2c.

For the regression of the experimental cure dataset to obtain the mechanical property parameters, it is necessary to calculate corresponding theoretical dispersion curves. These theoretical curves are derived from the Rayleigh-Lamb wave dispersion equations[12]:

$$\text{Symmetric modes:} \quad \frac{\tan(qh)}{\tan(ph)} = -\frac{4k^2qp}{\left(k^2-q^2\right)^2} \tag{2}$$

$$\text{Antisymmetric modes:} \quad \frac{\tan(qh)}{\tan(ph)} = -\frac{\left(k^2-q^2\right)^2}{4k^2qp} \tag{3}$$

with

$$p^2 = (\omega^2 / c_L^2) - k^2, \tag{4}$$

$$q^2 = (\omega^2 / c_S^2) - k^2, \tag{5}$$

and we also have:

$$c_L = c_S\sqrt{\frac{2(1-\upsilon)}{1-2\upsilon}}. \tag{6}$$

Here, the angular velocity $\omega = 2\pi f$. f is the frequency. h is the half thickness of the testing plate, k is the wavenumber, c_L is the longitudinal wave velocity of the testing material, c_s is the shear wave velocity, and υ is the Poisson's ratio. Take eq. (6) to eq. (4), then take eq. (4) and (5) into eq. (2) and (3). It can be concluded that the Lamb wave dispersion curves are frequency-wavenumber functions related to c_s and υ.

2.3 Dispersion curve regression

The least squares method is a commonly used optimization algorithm that can quickly find the best function match for data [17,18]. To accurately determine the shear wave velocity (c_S) and Poisson's ratio (ν) from experimental dispersion curves, we employed a nonlinear least squares optimization approach. The least square method is used to search the theoretical database $k_{\text{theo}}(c_S, \nu, f_i)$, obtained from the eq. (2) to eq. (6), in order to find the theoretical dispersion curve $k^{\text{opt}}(f)$ that best matches the experimental data $k_{\text{exp},fi}$, as well as the shear wave velocity c_S and Poisson's ratio ν corresponding to the best-match theoretical dispersion curve. The dispersion curve comparison process can be expressed as[14]:

$$c_S^{\,opt}, \nu^{opt} = \arg\min_{c_S,\nu} \sum_{i=1}^{N} \left[k_{\text{exp},f_i} - k_{\text{theo}}(c_S, \nu, f_i)\right]^2 \tag{7}$$

In the equation, the k_{exp} is the experimental wavenumber at i^{th} frequency, and the k_{theo} is the calculated theoretical wavenumber at i^{th} frequency with specific c_S and ν. After optimization, by analyzing the Lamb wave's dispersion relation using the aforementioned method, we can characterize the shear wave velocity and Poisson's ratio of the tested metal panel.

3. EXPERIMENT VALIDATION

To validate our method, we fabricated a stainless-steel panel using an SLM (Selective Laser Melting) metal 3D printer. A proof-of-concept experiment was subsequently conducted on the panel using our PZT-LDV sensing system to capture the time-space wavefield of Lamb waves. To measure the mechanical properties of the specimen, we analyzed the collected wavefields using our frequency-wavenumber analysis method, as described in **Section 2**. After that, we performed curve regression on the resulting multi-directional frequency-wavenumber spectra.

3.1 Experiments with an additive-manufactured 3D-printed stainless-steel plate

The test panel was 3D printed using a Renishaw AM 400 additive manufacturing system (Renishaw, USA) with 316L stainless-steel powder. The printed size is 180 × 160 × 6 mm and post-processed to a uniform thickness of 5 mm using a surface grinder. The material's density is approximately 7870 kg/m³.

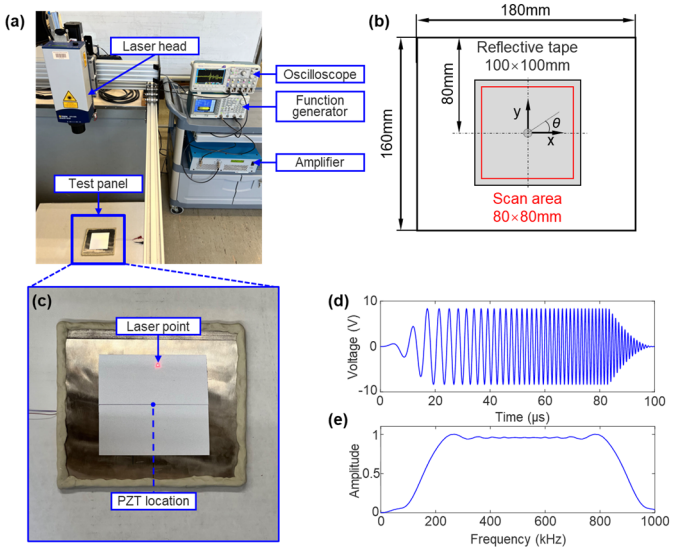

FIGURE 3: EXPERIMENTAL SETUP AND SCANNING SCHEMATIC REPRESENTATION OF THE TEST SPECIMEN

Figures 3a, 3b, and 3c illustrate the experimental setup, a schematic of the specimen layout, and a zoomed view of the test

© 2024 by ASME

board with reflective tape, respectively. The stainless-steel panel was fabricated with the following printing parameters: a laser power of 350W, a layer thickness of 30 μm, a travel speed of 1000 mm/min, a hatch spacing of 50 μm, and a hatch rotation angle of 67 degrees. To non-destructively excite Lamb waves in the test plate, a 7 mm diameter piezoelectric actuator was affixed to the back surface of the test panel, with its center position designated as the coordinate origin. The x-axis of the test panel was aligned parallel to the x-axis of the printing coordinate system. The angle θ represents the angle between the desired testing line and the positive x-axis.

The PZT actuator was driven by an arbitrary waveform function generator (AFG3052C, Tektronix, USA), producing a 50–1000 kHz Hanning-windowed chirp burst. This signal was amplified to 15 Vpp (Voltage peak to peak) using a voltage amplifier (A075, E&I, USA) (Figures 3d and 3e). An LDV (OFV-505, Polytec, Germany) measured the out-of-plane displacement component of the Lamb waves to capture the time-space wavefield over an 80 mm × 80 mm scanning grid. The grid had a 0.8 mm interval, resulting in a total of 10,201 scanning points (101 × 101). The acquisition sampling frequency was set to 31.25 MHz.

3.2 LDV scanning result and frequency-wavenumber analysis

With the LDV measurement, figures 4a to 4d show the time-space wavefield at 40, 50, 60, and 70 μs, respectively.

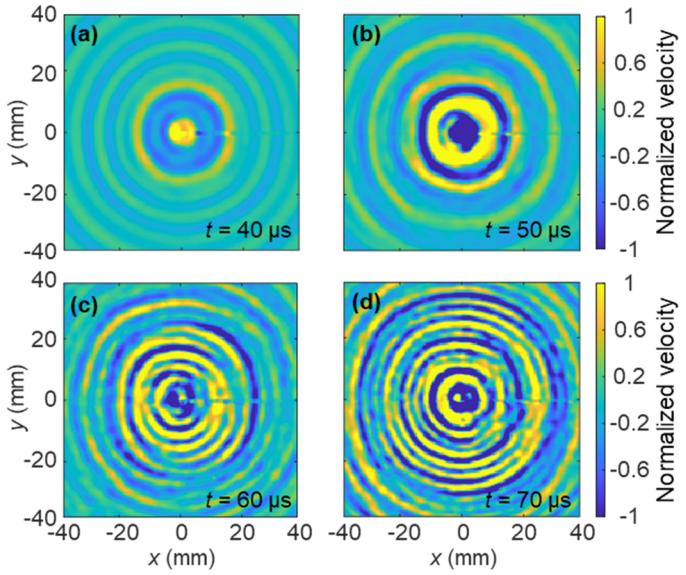

FIGURE 4: ACQUIRED TIME-SPACE WAVEFIELD IN DIFFERENT TIMES.

Employing the method introduced in **Section 2.2**, frequency-wavenumber analysis was performed on the measured wavefields, resulting in a stack of wavenumber spectra at various frequencies, as displayed in Figures 5a to 5d. Reference wavenumber curves for the A0 mode (shown as a blue dashed line) were plotted to aid in identifying variations in wavenumber across different directions. By comparing the A0 mode's wavenumber spectra with these reference curves, it was observed that the wavenumbers vary by angle θ. This variation is likely attributed to the 3D printing orientation of the tested panel.

For extracting the frequency-wavenumber spectrum in a specific degree from the wavenumber spectra, the coordinate system of the spectrum was converted to a polar coordinate system. The origin ($x = 0$, $y = 0$) was converted to ($\rho = 0$), and θ is the desired testing direction. In this study, the common testing angles, θ = 0, 45, 60, and 90 degrees, were selected, and the wavenumber amplitudes at different frequencies, ranging from 50 kHz to 1MHz, were extracted and plotted as multi-directions wavenumber-frequency spectra (Fig. 5e to 5h).

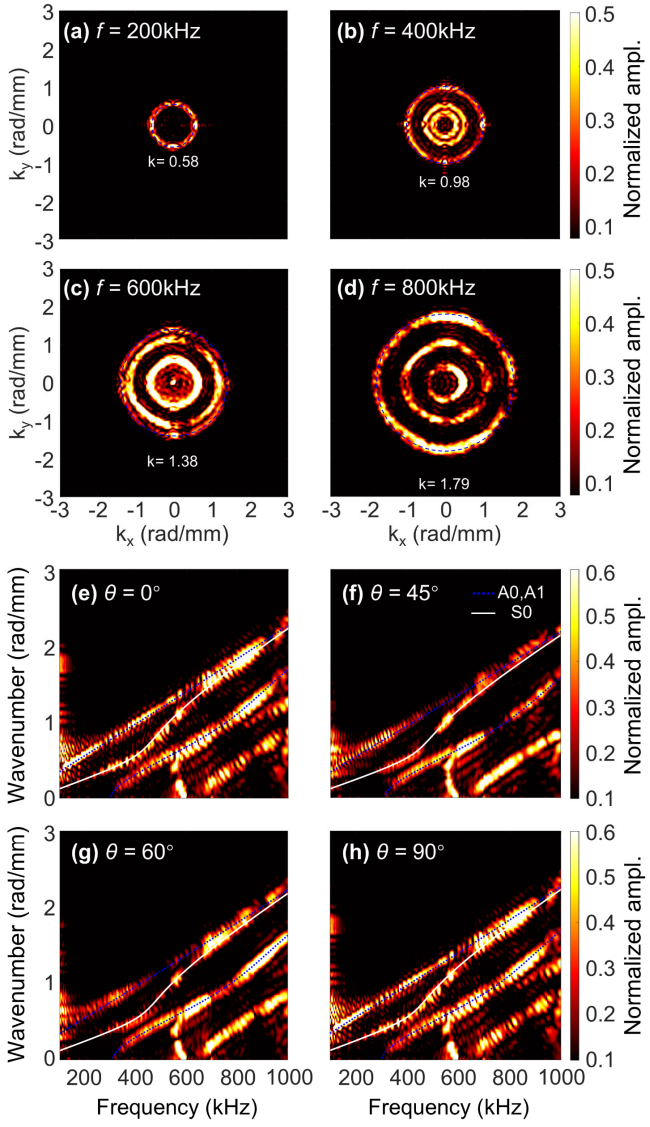

FIGURE 5: WAVENUMBER SPECTRA IN DIFFERENT FREQUENCIES AND DISPERSION CURVE REGRESSION RESULTS WITH DIFFERENT DIRECTIONS OF TESTED 316L PANEL.

For regression accuracy, the metal's Poisson's ratio and shear wave velocity are assumed to range from 0.24 to 0.30 and 2700m/s to 3300m/s, respectively [19,20]. After marking the A0

© 2024 by ASME

mode's highest amplitude at different frequencies for each θ, the least square regression was performed using our customized MATLAB code worked with MATLAB Curve Fitting Toolbox, employing theoretical equations introduced in **Section 2.3** to do regression for the experimental frequency and wavenumber data and find all theoretical dispersion curves best matching the experimental results, along with corresponding mechanical material parameters (υ and c_s). The results for selected θ are displayed in Table 1.

TABLE 1: EXPERIMENTAL MECHANICAL PROPERTIES FOR DIFFERENT θ

θ (°)	υ	c_s (m/s)
0	0.255	3060.28
45	0.260	3103.34
60	0.257	3090.73
90	0.252	3022.26

Clearly, both the shear wave velocity and Poisson's ratio vary with θ, with the lowest shear wave velocity observed at θ=90 degrees. This phenomenon aligns with the known mechanical performance characteristics of 3D printed products, where the structure typically exhibits weaker performance along the bonding direction.

3.3 Experiments and results with a 2024 T3 Aluminum Panel

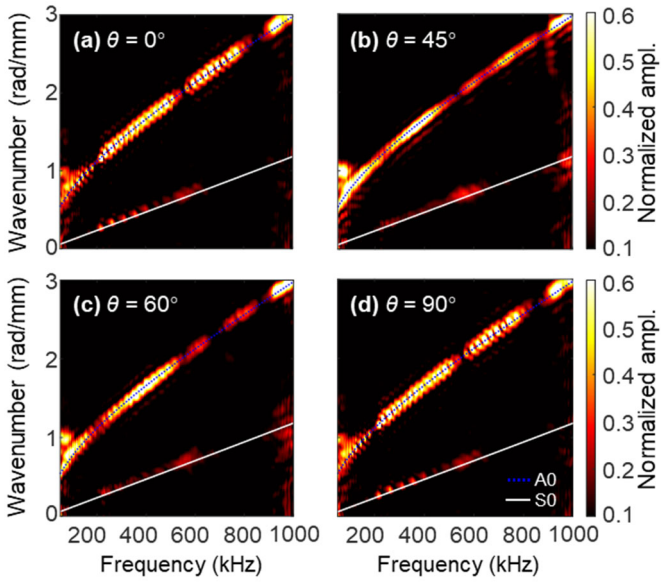

FIGURE 6: CURVE REGRESSION RESULT WITH DIFFERENT DIRECTIONS OF THE 2024-T3 ALUMINUM PLATE.

Traditional tensile and compression tests are often unreliable for 3D printed products due to their anisotropic nature and common defects such as voids and delamination. To validate the accuracy of our method, we tested a standard 0.75 mm thick 2024-T3 aluminum plate, which is isotropic, resulting in minimal directional differences in properties (Fig. 6). After averaging the mechanical properties from different directions, we obtained a shear wave velocity (c_s) of 3159.12 m/s and a Poisson's ratio (v) of 0.331, very close to the value by ASTM standards. The testing results confirm that our sensing system and wavenumber analysis method effectively characterize the mechanical properties of plate structures.

4. CONCLUSION

This article developed a non-destructive characterization method that integrates the PZT-LDV Lamb wave sensing system with a multi-directional frequency-wavenumber analysis technique to characterize the mechanical properties (shear wave velocity and Poisson's ratio) in multiple directions of metal plate fabricated through additive manufacturing. The experimental results demonstrate the precision and reliability of our method. We hope that this approach will provide an effective solution for enhancing the manufacturing processes and quality control in the field of metal additive manufacturing.

ACKNOWLEDGEMENTS

The authors would like to thank the financial support from the National Science Foundation (CMMI-2243771 and CMMI 2340016), DOE Office of Nuclear Energy's Nuclear Energy University Programs (DE-NE0009187), National Aeronautics and Space Administration (MS-80NSSC22M0273), and Federal Aviation Administration (FAA 12-C-AM-MSU).

REFERENCES

[1] M. Armstrong, H. Mehrabi, and N. Naveed, "An overview of modern metal additive manufacturing technology," *Journal of Manufacturing Processes* **84**, 1001–1029, 2022.

[2] Y. Kok, X. P. Tan, P. Wang, M. L. S. Nai, N. H. Loh, E. Liu, and S. B. Tor, "Anisotropy and heterogeneity of microstructure and mechanical properties in metal additive manufacturing: A critical review," *Materials & Design* **139**, 565–586, 2018.

[3] A. du Plessis, I. Yadroitsava, and I. Yadroitsev, "Effects of defects on mechanical properties in metal additive manufacturing: A review focusing on X-ray tomography insights," *Materials & Design* **187**, 108385, 2020.

[4] L. Yang, B. Cai, R. Zhang, K. Li, Z. Zhang, J. Lei, B. Chen, and R. Wang, "Mechanical Analysis and Performance Optimization for the Lunar Rover's Vane-Telescopic Walking Wheel," *Engineering* **6**, 936–943, 2020.

[5] Y. Du, Z. Pei, L. Shen, J. Li, B. Cai, T. Li, L. Bo, and Z. Tian, "Acoustic streaming effects on collagen self-assembly," in *Health Monitoring of Structural and Biological Systems XVIII* **12951**, (SPIE, 2024).

[6] T. DebRoy, H. L. Wei, J. S. Zuback, T. Mukherjee, J. W. Elmer, J. O. Milewski, A. M. Beese, A. Wilson-Heid, A. De, et al., "Additive manufacturing of metallic components – Process, structure and properties," *Progress in Materials Science* **92**, 112–224, 2018.

[7] M. C. Sow, T. De Terris, O. Castelnau, Z. Hamouche, F. Coste, R. Fabbro, and P. Peyre, "Influence of beam diameter on Laser Powder Bed Fusion (L-PBF) process," *Additive Manufacturing* **36**, 101532, 2020.

© 2024 by ASME

[8] S. L. Sing and W. Y. Yeong, “Laser powder bed fusion for metal additive manufacturing: perspectives on recent developments,” *Virtual and Physical Prototyping* **15**, 359–370, 2020.
[9] F. Dababneh and H. Taheri, “Investigation of the influence of process interruption on mechanical properties of metal additive manufacturing parts,” *CIRP Journal of Manufacturing Science and Technology* **38**, 706–716, 2022.
[10] J. J. Lewandowski and M. Seifi, “Metal Additive Manufacturing: A Review of Mechanical Properties,” *Annual Review of Materials Research* **46**, 151–186, 2016.
[11] T. D. Ngo, A. Kashani, G. Imbalzano, K. T. Q. Nguyen, and D. Hui, “Additive manufacturing (3D printing): A review of materials, methods, applications and challenges,” *Composites Part B: Engineering* **143**, 172–196, 2018.
[12] V. Giurgiutiu, *Structural health monitoring with piezoelectric wafer active sensors*, 2008.
[13] Z. Tian and L. Yu, “Lamb wave frequency–wavenumber analysis and decomposition,” *Journal of Intelligent Material Systems and Structures* **25**, 1107–1123, 2014.
[14] B. Cai, T. Li, L. Bo, J. Li, R. Sullivan, C. Sun, W. Huberty, and Z. Tian, “Development of a piezo stack – laser doppler vibrometer sensing approach for characterizing shear wave dispersion and local viscoelastic property distributions,” *Mechanical Systems and Signal Processing* **214**, 111389, 2024.
[15] B. Cai, L. Shen, Z. Pei, T. Li, J. Li, L. Bo, Y. Du, and Z. Tian, “Development of a Laser Vibrometer-Based Shear Wave Sensing System for Characterizing Mechanical Properties of Viscoelastic Materials,” 27 November 2023, *American Society of Mechanical Engineers Digital Collection*.
[16] Z. Tian, W. Xiao, Z. Ma, and L. Yu, “Dispersion curve regression – assisted wideband local wavenumber analysis for characterizing three-dimensional (3D) profile of hidden corrosion damage,” *Mechanical Systems and Signal Processing* **150**, 107347, 2021.
[17] X. Chen, Z. Wang, X. Zhang, R. Fu, D. Wang, M. Zhang, and H. Wang, “Deep Autoencoder Imaging Method for Electrical Impedance Tomography,” *IEEE Transactions on Instrumentation and Measurement* **70**, 1–15, 2021.
[18] Z. Wang, X. Zhang, D. Wang, R. Fu, X. Chen, and H. Wang, “Shape Reconstruction for Electrical Impedance Tomography with V2D-Net Deep Convolutional Neural Network,” in *2022 IEEE International Instrumentation and Measurement Technology Conference (I2MTC)*, (2022).
[19] N. Huang, O. J. Cook, R. L. W. Smithson, C. M. Kube, A. P. Argüelles, and A. M. Beese, “Use of ultrasound to identify microstructure-property relationships in 316 stainless steel fabricated with binder jet additive manufacturing,” *Additive Manufacturing* **51**, 102591, 2022.
[20] E. Garlea, H. Choo, C. C. Sluss, M. R. Koehler, R. L. Bridges, X. Xiao, Y. Ren, and B. H. Jared, “Variation of elastic mechanical properties with texture, porosity, and defect characteristics in laser powder bed fusion 316L stainless steel,” *Materials Science and Engineering: A* **763**, 138032, 2019.

© 2024 by ASME